

Rapid measurement of heteronuclear transverse relaxation rates using non-uniformly sampled $R_{1\rho}$ accordion experiments

Sven Wernersson¹, Göran Carlström², Andreas Jakobsson³, Mikael Akke^{1,*}

¹ Biophysical Chemistry, Center for Molecular Protein Science, Department of Chemistry, Lund University, Box 124, SE-22100 Lund, Sweden

² Centre for Analysis and Synthesis, Department of Chemistry, Lund University, Box 124, SE-22100 Lund, Sweden

³ Department of Mathematical Statistics, Lund University, Box 118, SE-22100 Lund, Sweden

Correspondence to: Mikael Akke (mikael.akke@bpc.lu.se)

Abstract. Multidimensional, heteronuclear NMR relaxation methods are used extensively to characterize the dynamics of biological macromolecules. Acquisition of relaxation datasets on proteins typically require significant measurement time, often several days. Accordion spectroscopy offers a powerful means to shorten relaxation rate measurements by encoding the ‘relaxation dimension’ into the indirect evolution period in multidimensional experiments. Time savings can also be achieved by nonuniform sampling (NUS) of multidimensional NMR data, which is used increasingly to improve spectral resolution or increase sensitivity per unit time. However, NUS is not commonly implemented in relaxation experiments, because most reconstruction algorithms are inherently nonlinear, leading to problems when estimating signal intensities, relaxation rate constants and their error bounds. We have previously shown how to avoid these shortcomings by combining accordion spectroscopy with NUS, followed by data reconstruction using sparse exponential mode analysis, thereby achieving a dramatic decrease in the total length of longitudinal relaxation experiments. Here, we present the corresponding transverse relaxation experiment, taking into account the special considerations required for its successful implementation in the framework of the accordion-NUS approach. We attain the highest possible precision in the relaxation rate constants by optimizing the NUS scheme with respect to the Cramér-Rao lower bound of the variance of the estimated parameter, given the total number of sampling points and the spectrum-specific signal characteristics. The resulting accordion-NUS $R_{1\rho}$ relaxation experiment achieves comparable precision in the parameter estimates, compared to conventional CPMG R_2 or spin-lock $R_{1\rho}$ experiments, while saving an order of magnitude in experiment time.

1 Introduction

NMR relaxation offers a powerful means to study the dynamics of proteins and other biological macromolecules (Alderson and Kay, 2020; Mittermaier and Kay, 2009; Palmer, 2004). Most commonly, relaxation experiments on proteins are acquired as a series of two-dimensional (2D) spectra, in order to resolve as many resonances as possible, wherein relaxation rates are measured via their effect on the resonance intensities in a ‘third dimension’ obtained by parametrically varying the length of a relaxation time period or the refocusing frequency of an applied radio-frequency field, or both. Thus, relaxation experiments

often involve significant time requirements, and may take up to several days. An ingenious alternative to these lengthy experiments is offered by the accordion approach originally developed by Bodenhausen & Ernst (Bodenhausen and Ernst, 1981, 1982) to study chemical exchange. In accordion spectroscopy, the ‘third dimension’ is incremented synchronously with the second (indirect) dimension, with the result that the relaxation decay is encoded into the interferogram of the indirect evolution period. Consequently, the total experiment time is reduced significantly. More recent implementations include the constant-time accordion experiment (Carr et al., 1998; Mandel and Palmer, 1994), from which relaxation rate constants can be extracted using either time-domain analysis of the interferogram (Mandel and Palmer, 1994), or lineshape analysis of the Fourier-transformed data (Chen and Tjandra, 2009; Harden and Frueh, 2014; Rabier et al., 2001).

Nonuniform sampling (NUS) of the indirect dimensions of multidimensional NMR data can greatly shorten the total experiment time (Gołowicz et al., 2020; Mobli and Hoch, 2014), and has become commonplace in the last decade. However, most spectral reconstruction algorithms suffer from nonlinearity of signal intensities, which limits ‘plug-and-play’ use of NUS in quantitative experiments, and requires careful consideration of both sampling schemes and data modeling to produce consistent results and reliable error estimates (East et al., 2021; Linnet and Teilum, 2016; Mayzel et al., 2017; Stetz and Wand, 2016; Urbańczyk et al., 2017). We recently introduced an approach that avoids these problems by combining accordion spectroscopy with NUS (Carlström et al., 2019), and analyzing the resulting data using DSURE (damped super-resolution estimator), a sparse reconstruction technique enabling maximum-likelihood estimation of the time-domain signal parameters from NUS data (Juhlin et al., 2018; Swärd et al., 2016). We stress the point that accordion spectroscopy encodes the desired relaxation rate constants in the interferogram of the multidimensional data set, and hence the analysis does not rely on measuring intensities in multiple NUS datasets. Moreover, maximum likelihood estimation of model parameters makes it straightforward to derive reliable error bounds. Our approach leads to accumulated time savings through both the accordion and NUS methods. Compared to a conventional relaxation experiment, accordion reduces the experiment time by a factor of $M/2$, where M is the number of datasets included in the conventional approach, and NUS reduces the experiment time by a factor of N_{full}/N , where N_{full} is the number of data points sampled in the indirect dimension of the conventional experiment and N is the number of points in the NUS scheme. We previously demonstrated this approach by measuring longitudinal relaxation rate constants (R_1) in proteins with time savings of up to a factor of 20 (Carlström et al., 2019). For example, using this approach we have successfully measured R_1 on protein samples with 10-fold lower concentration than normally used (Verteramo et al., 2021).

A number of considerations are of general importance when choosing the detailed sampling scheme for NUS, including the need to keep the total number of increments small in order to speed up data acquisition, to sample short t_1 values to optimize sensitivity and long t_1 values to optimize spectral resolution (Hyberts et al., 2014; Mobli and Hoch, 2014). Various NUS schemes have been developed to accommodate these different requirements, including the popular Poisson-gap scheme (Hyberts et al., 2010). However, in the context of relaxation experiments, the most important aspect is to achieve high precision in the estimated relaxation rate constants. To this end, we have previously developed a method to optimize the sampling scheme with respect to the Cramér-Rao lower bound (CRLB), which yields a lower bound on the achievable variance of the parameters,

65 given the actual spectrum characteristics (i.e., the total number of component signals and their resonance frequencies, linewidths, and intensities) and the number of sampling points (Carlström et al., 2019; Månsson et al., 2014; Swärd et al., 2018); similar implementations have followed (Jameson et al., 2019; Waudby et al., 2021).

Here, we introduce accordion-NUS $R_{1\rho}$ pulse sequences that complement the previously presented R_1 experiment (Carlström et al., 2019). The $R_{1\rho}$ relaxation experiment can be implemented using either on-resonance or off-resonance spin-
 70 lock fields, making it suitable for measurement of R_2 relaxation rate constants to characterize fast dynamics, as well as conformational/chemical exchange processes across a wide range of timescales (Akke and Palmer, 1996). The present paper addresses several issues concerning measurement of transverse relaxation rates in accordion mode combined with NUS. We validate the accordion-NUS method by extensive comparisons with data acquired using uniformly sampled accordion experiments, as well as conventional non-accordion experiments of both the $R_{1\rho}$ and CPMG R_2 types. In addition, exchange
 75 contributions to the transverse relaxation rates were characterized using CPMG relaxation dispersion experiments. Our results show that the accordion-NUS $R_{1\rho}$ experiment enables measurement of accurate R_2 relaxation rate constants with a relative uncertainty of only 2–3% using a sampling density of 50% in the indirect dimension. Lower sampling densities lead to progressively reduced precision, with 5% relative uncertainty being obtained using less than 20% sampling density.

2 Materials and Methods

80 2.1 Constant-time accordion relaxation methodology

For completeness, here we briefly outline the salient features of the constant-time accordion method (Mandel and Palmer, 1994). Figure 1 shows the accordion $R_{1\rho}$ pulse sequence. The total relaxation delay is $T_\kappa = n \cdot 4 \cdot \tau$, where n is the sampled point number in t_1 , $\tau = (\kappa \Delta t_1)/4$, Δt_1 is the dwell time, and κ is the accordion scaling factor. The total constant-time delay $T = \tau_1 + \tau_2 + \tau_3$, where $\tau_1 = (T - t_1)/2$, $\tau_2 = T/2 - \Delta$, $\tau_3 = \Delta + t_1/2$, $\Delta = 1/(4J)$, and J is the ^1H - ^{15}N 1J -coupling constant ($\sim 92\text{Hz}$). The
 85 constant-time evolution period leads to reduced signal-to-noise compared to the non-constant time alternative, but is still favorable due to its superior resolution of closely spaced signals (Mandel and Palmer, 1994), which is of critical importance in accordion experiments (see Results). In the forward accordion experiment, where T_κ is incremented together with t_1 , the effective relaxation rate constant of the interferogram is given by: $R_{2,\text{fwd}} = R_{\text{inh}} + \kappa R_{1\rho}$, where R_{inh} describes line-broadening due to static magnetic field inhomogeneity. In the reverse accordion experiment, where T_κ is decremented as t_1 is incremented,
 90 the effective relaxation rate constant of the interferogram is given by: $R_{2,\text{rev}} = R_{\text{inh}} - \kappa R_{1\rho}$. The rotating-frame relaxation rate constant is calculated as: $R_{1\rho} = (R_{2,\text{fwd}} - R_{2,\text{rev}})/(2\kappa)$. As an alternative, $R_{1\rho}$ can also be determined by subtracting from $R_{2,\text{fwd}}$ the linewidth measured in an interferogram from a reference experiment with the relaxation period set to 0: $R_{1\rho} = (R_{2,\text{fwd}} - R_{\text{ref}})/\kappa$. In estimating the standard error of $R_{1\rho}$ by error propagation, the factor of 2 difference in the numerator of the alternative approaches offsets the higher signal-to-noise in the reference experiment, as compared to the reverse experiment, with the
 95 result that the error bars are actually lower in the forward-reverse accordion approach.

2.2 NMR sample preparation

Uniformly ^{15}N -enriched galectin-3C was expressed and purified as described previously (Diehl et al., 2009, 2010; Wallerstein et al., 2021). The NMR sample containing galectin-3C in complex with the ligand 3'-[4-(3-fluorophenyl)-1H-1,2,3-triazol-1-yl]-3'-deoxy- β -D-galactopyranosyl-1-thio- β -D-glucopyranoside was prepared as described (Wallerstein et al., 2021) to yield a final protein concentration of 0.9 mM in 5 mM HEPES buffer, pH 7.3.

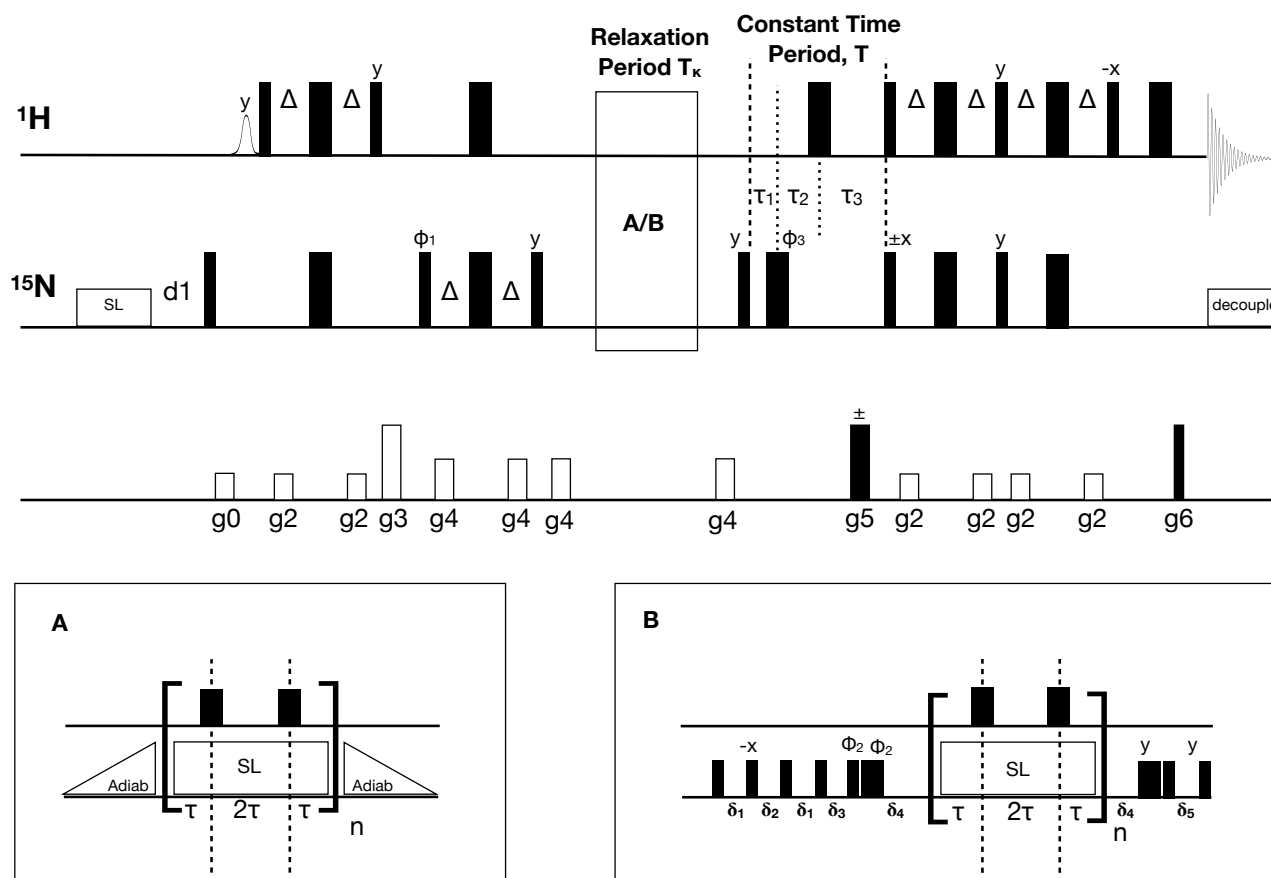


Figure 1. Pulse sequence for the ^1H -detected accordion-NUS ^{15}N $R_{1\rho}$ spin-lock experiment. Thin (thick) black bars correspond to 90° (180°) non-selective pulses. All pulses have phase x, unless otherwise indicated. The spin-lock at the beginning of the sequence is a heat-compensation block (Wang and Bax, 1993). The open bell-shaped pulse at the beginning of the sequence is a selective pulse on the water resonance (Grzesiek and Bax, 1993). INEPT polarization transfer steps (Bodenhausen and Ruben, 1980; Morris and Freeman, 1979) use $\Delta = 1/(4J_{\text{HN}})$, where J_{HN} is the one-bond scalar coupling constant. The relaxation period can be run with (A) adiabatic ramps, or with (B) hard-pulse alignment blocks (Hansen and Kay, 2007). In both cases, 180° ^1H pulses are present at time points τ and 3τ to suppress cross-correlated relaxation (Massi et al., 2004). The hard pulse alignment delays are $\delta_1 = 1/(2\omega_{\text{SL}}) - 2/\omega_{\text{N}}$, $\delta_2 = \delta' \omega_{\text{SL}} - 2/\omega_{\text{N}}$, $\delta_3 = \delta'(2\omega_{\text{SL}}) - 2/\omega_{\text{N}}$, $\delta_4 =$

110 $1/\omega_N$, $\delta_S = 1/(2 \omega_{SL}) - 2/\omega_N$ where ω_N is the field strength of the high power ^{15}N 90-degree pulse, ω_{SL} is the spin-lock field strength, and $\delta = 1.35$ is a scaling factor optimized for alignment of spins with offsets within $\pm\omega_{SL}$. The total relaxation delay $T_k = n \cdot 4 \cdot \tau$, where n is the sampled point number in t_1 , and $\tau = (\kappa \Delta t_1)/4$, with $\kappa = 3$. The total constant-time period $T = \tau_1 + \tau_2 + \tau_3 = 70$ ms, where $\tau_1 = (T - t_1)/2$, $\tau_2 = T/2 - \Delta$, and $\tau_3 = \Delta + t_1/2$. The phase cycle is $\phi_1 = (x, -x)$, $\phi_2 = 8(y), 8(-y)$, $\phi_3 = (x, x, y, y, -x, -x, -y, -y)$. The receiver phase cycle is $\text{rec} = (x, -x, -x, x, x, -x, -x, x)$ with relaxation block (A), and $\text{rec}, (-\text{rec})$ with block (B). Gradient enhanced PEP polarization transfer (Kay et al., 1992b; Palmer et al., 1991) is achieved by acquiring a second data set with inversion of the phase of the ^{15}N 90° pulse indicated with $\pm x$, and gradient g_5 . The gradients g_5 and g_6 are used for coherence selection. The phase ϕ_1 and the receiver phase are inverted for each t_1 increment. The gradient times and levels are g_0 : 1 ms, 8.9 G cm $^{-1}$; g_1 : 1ms, 8.9 G cm $^{-1}$; g_2 : 0.5 ms, 7.1 G cm $^{-1}$; g_3 : 1 ms, 44.4 G cm $^{-1}$; g_4 : 0.5 ms, 14.2 G cm $^{-1}$; g_5 : 1.25 ms, 53.2 G cm $^{-1}$; g_6 : 0.125 ms, 53.8 G cm $^{-1}$.

2.3 NMR relaxation experiments

120 All pulse sequences were based on the ^1H - ^{15}N HSQC format (Bodenhausen and Ruben, 1980). Conventional and accordion ^{15}N $R_{1\rho}$ experiments were acquired with uniform sampling (US) on an Agilent/Varian VNMRS 600 MHz instrument equipped with a 5 mm HCN triple-resonance room temperature probe. To allow comparisons between the two different ways of estimating $R_{1\rho}$ from accordion data, accordion experiments were performed using a combination of forward and reverse accordion modes (i.e., incrementing or decrementing the relaxation delay in step with t_1) together with a reference experiment
125 excluding the accordion relaxation period but including the alignment blocks (Fig. 1). Both the conventional and accordion $R_{1\rho}$ experiments were performed with two different methods for aligning the magnetization along the effective spin-lock field axis: either hard pulses and delays (Hansen and Kay, 2007) or adiabatic amplitude/frequency ramps with a tan/tanh profile of 1.8 ms duration (Mulder et al., 1998). In the former case, the scaling factor δ was set to 1.35 for optimum alignment of spins with offsets within $\pm\omega_{SL}$ from the spin-lock carrier frequency. The ^{15}N dimension was acquired with a spectral width of 2006
130 Hz, sampled over 132 increments in the accordion $R_{1\rho}$ experiment utilizing adiabatic alignment, with 128 increments in the accordion experiment using hard-pulse alignment, and with 128 increments in both conventional $R_{1\rho}$ experiments. The ^1H dimension was acquired with a spectral width of 8446 Hz, sampled over 2028 complex data points, in all experiments. All accordion experiments (forward, reverse, and reference) were acquired interleaved. Conventional $R_{1\rho}$ experiments were acquired by interleaving the relaxation periods of (6, 12, 23.9, 2×47.9, 95.7, and 191.4) ms. All $R_{1\rho}$ experiments employed a
135 spin-lock field strength of $\omega_{SL}/(2\pi) = 1380$ Hz. The effective spin-lock field strength in the rotating frame is given by $\omega_{\text{eff}} = (\omega_{SL}^2 + \Omega^2)^{1/2}$, where Ω is the offset from the spin-lock carrier (Akke and Palmer, 1996; Davis et al., 1994). The transverse relaxation constant R_2 was extracted from the $R_{1\rho}$ relaxation rates by correcting for off-resonance effects using the relationship $R_{1\rho} = \cos^2(\theta)R_1 + \sin^2(\theta)R_2$, where θ is the tilt angle of the spin-lock field defined by $\tan(\theta) = \omega_{SL}/\Omega$, and the previously determined R_1 rate constant.

140 Conventional R_1 and R_2 CPMG experiments (Farrow et al., 1995; Skelton et al., 1993) were acquired with uniform sampling on a Bruker NEO 600 MHz instrument equipped with a 5 mm HPCN QCI cryo-probe, using spectral widths of 2129 Hz, sampled over 128 increments, in the ^{15}N dimension and 9615 Hz, sampled over 2048 complex data points, in the ^1H dimension. The R_1 and R_2 relaxation periods were acquired interleaved with the t_1 increments using delays of (2×0.04, 0.08, 0.12, 0.2, 0.4, 2×0.6, 0.72, 2×0.8, 1.0, 1.2, 1.6, and 2.0) s and (0, 42.2, 2×84.5, 126.7, and 169.0) ms, respectively. The R_1

experiment utilized ^1H WALTZ decoupling during the relaxation period. The R_2 experiment employed CPMG pulse trains with a fixed refocusing frequency, $\nu_{\text{CPMG}} = 1/(2\tau_{\text{CPMG}}) = 625$ Hz, where τ_{CPMG} is the delay between 180° pulses in the CPMG train, and a 180° pulse length of $80\text{ }\mu\text{s}$. The R_2 values were not corrected for off-resonance effects. We also recorded CPMG relaxation dispersion datasets at static magnetic field strengths of 11.7 T and 14.1 T, using Agilent/Varian spectrometers equipped with 5 mm HCN triple-resonance room temperature probes. The relaxation dispersion experiment was run as a constant-time version (Mulder et al., 2001) of the relaxation-compensated CPMG pulse sequence (Loria et al., 1999), using 18 refocusing frequencies acquired interleaved with 128 t_1 increments covering spectral widths of 1550 Hz (2006 Hz) at 11.7 T (14.1 T). The experiments at 11.7 T and 14.1 T employed refocusing frequencies ν_{CPMG} of (2×0 , 2×50 , 2×100 , 2×150 , 2×200 , 250, 300, 400, 500, 600, 700, 750, and 950) Hz and (2×0 , 2×50 , 2×100 , 2×150 , 2×200 , 2×250 , 350, 450, 550, 700, 850, and 1000) Hz, respectively.

2.4 Nonuniform sampling schemes

NUS schemes were generated by selecting data points from the uniformly sampled accordion $R_{1\rho}$ dataset. CRLB optimized NUS schemes were obtained as described previously (Carlström et al., 2019). In practice, scheme optimization can be performed using modeled data constructed by taking known values of A_k , ω_k , and R_k obtained from DSURE estimation of an HSQC experiment, together with an estimate of the extra decay caused by relaxation during the accordion period (Carlström et al., 2019). Single-column CRLB optimized (col-opt) (Carlström et al., 2019; Swärd et al., 2018) and sine-weighted Poisson-gap (Hyberts et al., 2010) sampling schemes were implemented for the accordion $R_{1\rho}$ dataset with adiabatic ramps, using in-house MATLAB scripts. Poisson-gap sampling schemes were generated by randomly varying the argument of the sinusoidal weighting function between 0 and $\pi/2$; see (Hyberts et al., 2010). The best sampling scheme was identified as the one having the lowest sum of the CRLB calculated over all columns containing peaks. In the case of the col-opt approach, the selection was made among 97 different single-column CRLB optimized schemes corresponding to each slice of the interferogram containing protein signals, whereas in the case of Poisson-gap sampling 1000 different schemes were compared. The sampling scheme was optimized individually for each of the reference, forward, and reverse accordion experiments. In each case, we generated individual datasets sampled with $N = 22, 27, 32, 37, 42, 47, 52, 57, 62, 66, 67, 72, 77, 82, 87, 92, 97, 102, 107, 112, 117, 122$, or 127 increments in the indirect dimension. The NUS datasets resulting from the different sampling schemes were subsequently reconstructed using the DSURE algorithm.

2.5 Data reconstruction, processing, and analysis

Non-accordion (i.e., conventional) datasets were processed using NMRPipe (Delaglio et al., 1995), with forward linear prediction to double the number of data points, cosine-squared window apodization, and zero-filling to twice the size rounded to the nearest power of two. $R_{1\rho}$, R_1 , and R_2 relaxation rate constants were estimated from the conventional experiments by integrating the peak volumes using PINT (Ahlner et al., 2013; Niklasson et al., 2017), followed by fitting mono-exponential

decay functions to the volumes using in-house MATLAB scripts. The fitted R_2 values determined by CPMG experiments were not adjusted for off-resonance effects (Korzhnev et al., 2000). Standard errors were estimated using jackknife resampling (Mosteller and Tukey, 1977) as implemented in PINT. Standard errors in R_2 derived from $R_{1\rho}$ experiments were estimated by Monte-Carlo simulations using 10,000 samples drawn from normal distributions with widths corresponding to the standard errors of $R_{1\rho}$ and R_1 (Press et al., 1986).

The accordion datasets were processed and analyzed using the DSURE algorithm (Juhlin et al., 2018) implemented in MATLAB (The Mathworks, Inc.). DSURE reconstruction was performed on individual t_1 interferograms, as described previously (Carlström et al., 2019). DSURE models interferograms as sums of exponentially decaying sinusoids

$$A(t) = \sum_k^K A_k \exp[i\omega_k t - R_k t] + \varepsilon(t) \quad (1)$$

where A_k , ω_k , and R_k are the complex-valued amplitude, frequency, and decay rate of the k :th signal, respectively, $\varepsilon(t)$ represents additive noise, and the sum runs over all K signals identified in a given interferogram. In reconstructing accordion data, the time domain data from the reverse mode was inverted and complex conjugated before estimation using DSURE. Standard errors of the estimated parameters were calculated as the CRLB, which is very close to the RMSE for statistically efficient estimators like DSURE. Explicit comparison of the RMSE, calculated from Monte-Carlo simulations using 1000 samples, and the CRLB indicates that the two measures are in excellent agreement, and deviate by at most a factor of 1.6 for the worst case (an interferogram containing 3 signal maxima) among our 50% NUS data.

2.6 Statistical analysis

To compare the performance of the different approaches for measuring transverse relaxation rates, we used 4 different metrics. The relative difference and absolute deviation between datasets x and y are defined for a given residue i as $\Delta_{\text{rel}} = 2(x_i - y_i)/(x_i + y_i)$ and $\Delta_{\text{abs}} = |x_i - y_i|$, respectively. The RMSD between two datasets is calculated pairwise over all residues (N_{res}), $\text{RMSD} = [(\sum_i (x_i - y_i)^2 / N_{\text{res}})]^{1/2}$. The mean relative uncertainty of a given dataset is the mean, calculated over all residues, of the individual uncertainty in x_i (σ_{xi} ; one standard deviation, as estimated by the DSURE algorithm) divided by x_i , $\text{MRU} = (\sum_i \sigma_{xi}/x_i)/N_{\text{res}}$.

3 Results and Discussion

3.1 Pulse sequence design

The accordion-NUS $R_{1\rho}$ pulse sequence (Fig. 1) is based on our previous implementation to measure R_1 (Carlström et al., 2019), which included minor modifications of the original constant-time accordion experiment (Mandel and Palmer, 1994). In designing accordion-NUS versions of transverse relaxation experiments, it is necessary to consider the interplay between the minimum length of the relaxation block (A or B in Fig. 1), the number of sampled t_1 points, and the maximum attainable t_1 value. R_2 relaxation rate measurement is typically performed in one of two ways, using either CPMG pulse trains or a continuous spin-lock during the relaxation period, so as to maintain in-phase magnetization and avoid significant evolution

into anti-phase terms (Skelton et al., 1993), as well as reduce chemical/conformational exchange (R_{ex}) and magnetic-field inhomogeneity (R_{inh}) contributions to the effective transverse relaxation rate constant ($R_{2,\text{eff}}$). Furthermore, it is necessary to suppress the effects of cross-correlated relaxation, which amounts to introducing additional relaxation delays (Kay et al., 1992a; Palmer et al., 1992), and to mitigate the effects of off-resonance effects and pulse imperfections (Korzhnev et al., 2000), leading to extended phase cycles (Yip and Zuiderweg, 2004). CPMG-type experiments for measuring chemical exchange involve extended spin-echo elements to average the relaxation rates of in-phase and anti-phase coherences (Loria et al., 1999). All in all, these requirements typically lead to relatively long relaxation blocks in CPMG-based experiments. Since the accordion experiment increments (or decrements) the relaxation period synchronously with the t_1 period, the minimum incrementation step for the relaxation period limits the maximum number of points that can be acquired in the t_1 dimension. In our initial testing of CPMG-based accordion experiments to measure R_2 , we found that the maximum achievable length of the t_1 dimension was 64 points, before the duty cycle and relaxation losses became serious concerns. While the resulting resolution in t_1 might suffice in certain cases, we opted instead for increased flexibility and designed the transverse relaxation experiment based on a spin-lock period. This strategy allows for significantly shorter increments of the relaxation period, and further enables facile adaptation to off-resonance $R_{1\rho}$ experiments for conformational exchange measurement. We implemented two types of pulse sequence elements to align the magnetization along the effective spin-lock field: adiabatic amplitude/frequency ramps (Mulder et al., 1998), or an element comprising hard pulses and delays (Hansen and Kay, 2007). The hard-pulse element is shorter than the adiabatic ramp (0.25–0.45 ms versus 1.8 ms in the present case), and in principle reduces relaxation losses, while the adiabatic ramp achieves superior alignment over a wider range of offsets, making it suitable for off-resonance $R_{1\rho}$ experiments used to characterize chemical exchange processes.

3.2 Comparison of DSURE-modeled accordion $R_{1\rho}$ relaxation data and conventional relaxation data

The ^1H - ^{15}N 2D spectrum resulting from the accordion $R_{1\rho}$ relaxation data reconstructed using DSURE is shown in Fig. A1, together with representative examples of DSURE models of interferograms. We compared the performance of the accordion $R_{1\rho}$ experiments acquired with the two different alignment elements (adiabatic vs hard-pulse, see section 2.3), and also compared the results obtained using the two different combinations of accordion modes (forward–reverse vs forward–reference, see section 2.1). To validate the accordion $R_{1\rho}$ values determined using DSURE, we first compared these with rate constants determined from the conventional $R_{1\rho}$ experiment and the R_2 CPMG experiment (Fig. 2). Figure 2 shows the results obtained using the forward–reverse accordion data and adiabatic alignment, while the corresponding data obtained using hard-pulse alignment is highly similar and shown in Fig. A2. In general, the results are in very good agreement, with very few residues showing statistically significant deviations between experiments (Figs. 2a–d). Comparing the accordion $R_{1\rho}$ values with the conventional data, we obtain an RMSD of 0.45 s^{-1} , whereas the comparison with the CPMG data yields an RMSD of 0.59 s^{-1} . The CPMG data were not corrected for off-resonance effects (Korzhnev et al., 2000), leading to offset-dependent systematic errors of up to 5% that might explain the somewhat poorer agreement in this case. The distributions of relative

differences are centered around the mean values 0.02 s^{-1} and 0.00 s^{-1} , and are sharper than normal distributions (Figs. 2e, f). The means of relative differences should be compared with the average relative uncertainties of the estimated $R_{1\rho}$ values, which are 0.14 s^{-1} for the conventional data and 0.21 s^{-1} for the accordion data, indicating that the accordion $R_{1\rho}$ experiment yields accurate data of comparable precision compared to the conventional experiment. The slight tendency towards higher R_2 values determined from the accordion experiment reflects small, but noticeable differences for a subset of residues (viz. residues 151, 154, 181, 182, and 184). Visual inspection of these peaks indicates that these differences are likely due to overlap problems, which are exacerbated by the additional line broadening present in accordion spectra. In principle this problem could be mitigated by optimizing the accordion scaling factor κ , or by acquiring data as a 3D experiment (Carr et al., 1998; Chen and Tjandra, 2009). For some residues, notably L219, the R_2 value from the reference CPMG data set is considerably higher (Fig. 2b), reflecting the different levels of residual exchange contributions to the transverse relaxation rate resulting from the different refocusing frequencies. The L219 peak has an offset of -572 Hz from the ^{15}N spin-lock carrier, which results in an effective spin-lock field of $\omega_{\text{eff}}/(2\pi) = 1494\text{ Hz}$, more than a factor two greater than the effective CPMG refocusing field (625 Hz) in the reference R_2 dataset. L219 also shows clear signatures of fast conformational exchange in CPMG relaxation dispersion experiments (Fig. A3).

The two alignment variants yield highly similar results in the context of the accordion experiment, and the same is true for the two combinations of accordion modes (Fig. A4). The RMSD between the two alignment variants is 0.19 s^{-1} and the mean relative difference is 0.0 s^{-1} , and the corresponding numbers for the two combinations of accordion modes are 0.24 s^{-1} and 0.0 s^{-1} , respectively. In the following presentation of accordion-NUS experiments, we will base all analyses on the results obtained from the forward–reverse accordion approach using data acquired with adiabatic alignment.

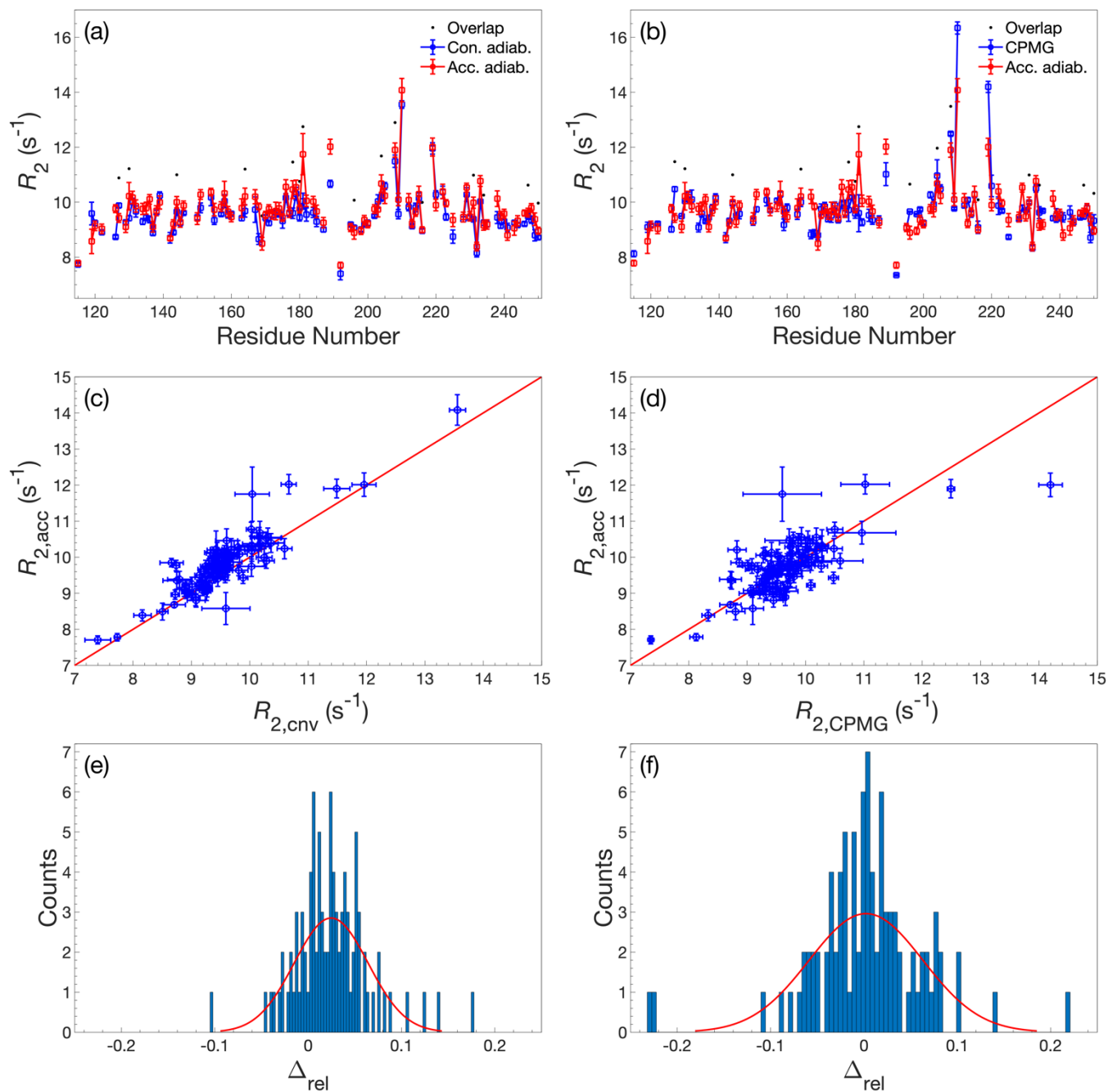


Figure 2. Comparison of R_2 determined by accordion $R_{1\rho}$ or conventional relaxation experiments. R_2 values determined by accordion $R_{1\rho}$ (red) spin-lock experiments compared with (a, c, e) R_2 determined by conventional $R_{1\rho}$ (blue) and (b, d, f) R_2 determined by conventional R_2 CPMG (blue). Both $R_{1\rho}$ experiments were acquired with adiabatic ramps. (a, b) R_2 plotted versus residue number. Black dots indicate residues showing significant overlap in the ^1H - ^{15}N HSQC spectrum. (c, d) Covariance plot of R_2 datasets. (e, f) Histogram of the relative differences between datasets. The red curve describes the normal distribution that best fits the data. In panels (a–d), error bars indicate ± 1 SD.

3.3 Comparison of non-uniformly sampled and uniformly sampled accordion $R_{1\rho}$ relaxation data

Next, we tested the performance of the accordion $R_{1\rho}$ experiment acquired with NUS. We have previously evaluated the performance of various NUS schemes for the acquisition of accordion R_1 data, and found that superior results were obtained for schemes generated by column-wise optimization directly against the CRLB (denoted col-opt in the following) or schemes following the Poisson-gap distribution (Carlström et al., 2019). Therefore, we restrict our present comparisons to the performance of these two NUS schemes. Starting from the uniformly sampled accordion $R_{1\rho}$ dataset acquired with adiabatic ramps and the forward–reverse accordion mode (from here on denoted the US dataset), we generated two times two datasets, where we used either col-opt or Poisson-gap sampling schemes, both optimized for the forward accordion experiment alone (set F), or optimized individually for each of the forward and reverse experiments (set F+R). In a real case scenario, it is arguably more practical to perform the optimization on model data sets constructed by taking known values of A_k , ω_k , and R_k obtained from DSURE estimation of an HSQC experiment, together with an estimate of the extra decay imparted by the accordion period (Carlström et al., 2019). Thus, there is no need to first record a US accordion data set prior to optimizing the NUS scheme.

Figure 3 illustrates the performance of the accordion-NUS $R_{1\rho}$ experiment acquired with different NUS schemes (red and blue symbols) and optimization protocols (left- and right-hand columns). We compared the $R_{1\rho}$ values determined by accordion-NUS with those obtained from the accordion-US dataset. In general, the performance decreases with decreasing number of sampled points, as might be expected. The RMSD between the NUS and US datasets shows a clear trend towards higher values as the number of sampling points decrease, from less than 0.2 s^{-1} at N_{full} to $0.8\text{--}1.0 \text{ s}^{-1}$ at $N = 22$ or 18% sampling density (Figs. 3a, b). However, these plots show some degree of scatter, which reflects the random nature of the NUS schemes, where any given scheme with a lower number of points might yield lower RMSD than another scheme with higher number of points. By contrast, the mean relative uncertainty (MRU) in the estimated $R_{1\rho}$ parameter shows an essentially monotonous increase with decreasing number of points, from 2.2% at N_{full} to 5% at $N = 22$ (Figs. 3c, d). The increasing uncertainty is relatively modest down to about 50% sampling ($N = 66$), where MRU is c:a 2.8%, but beyond this point both the RMSD and the MRU start to increase more steeply. These results are rather similar for the Poisson-gap and col-opt optimized schemes, with a small advantage for col-opt schemes, especially in the case of the precision of the estimated parameters (Figs. 3c, d). However, greater improvements in precision are expected for relaxation rate constants of signals in interferograms whose sampling schemes have been individually optimized with respect to the CRLB, as shown previously (Carlström et al., 2019). Altogether, these results indicate that our present implementation of the accordion-NUS approach to measure $R_{1\rho}$ achieves equally good precision of the estimated relaxation rate constants as did our previously presented accordion-NUS R_1 experiment (Carlström et al., 2019). Furthermore, the sampling schemes optimized separately for each of the forward and reverse experiments (F+R) show a modest advantage in performance over F for low N , which might be expected (compare Fig. 3a with 3b, and Fig. 3c with 3d).

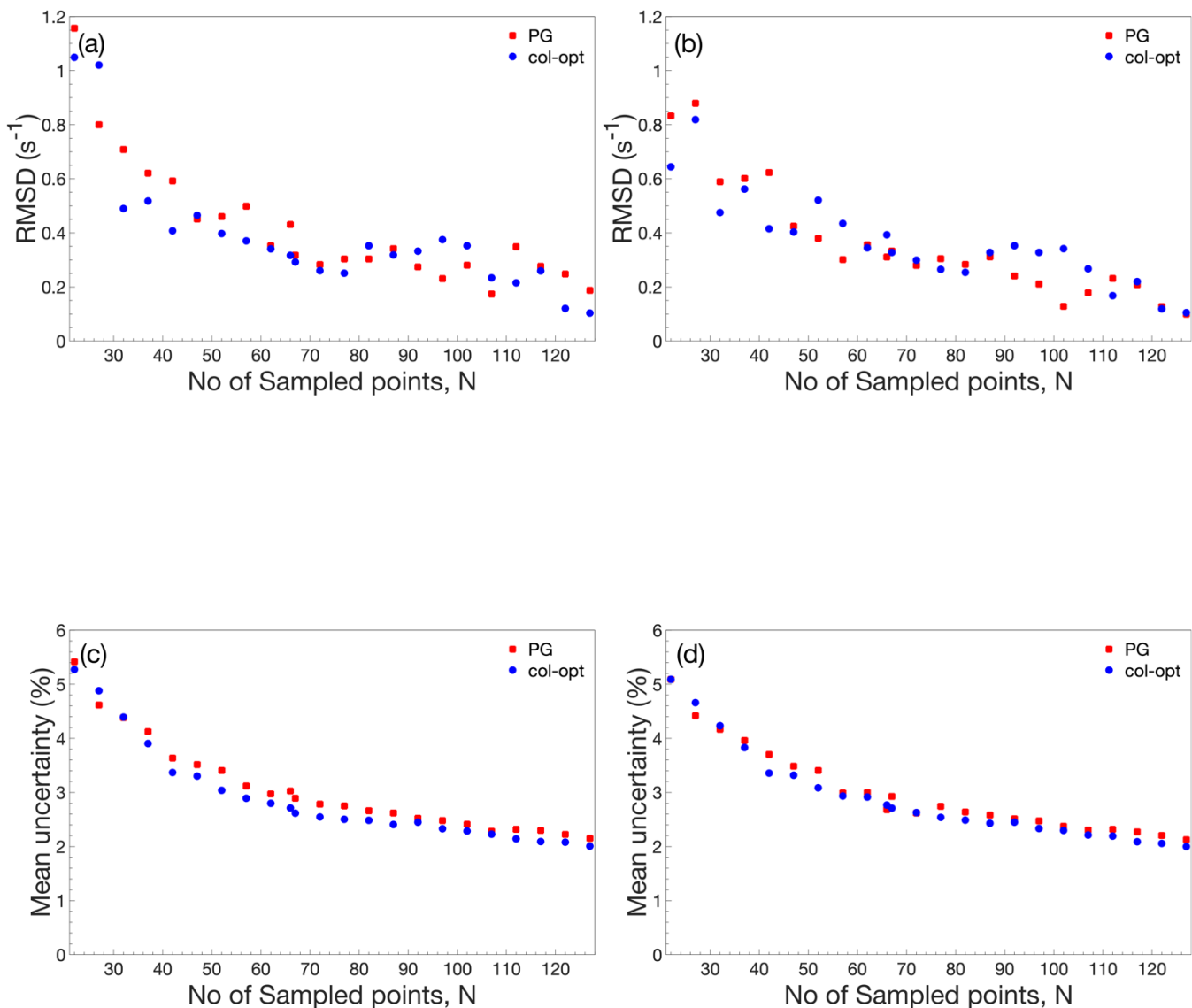


Figure 3. Performance comparison of accordion-NUS $R_{1\rho}$ experiments. (a, b) RMSD between the NUS dataset and the corresponding US dataset. (c, d) Mean relative uncertainty of the NUS $R_{1\rho}$ estimates. The left-hand panels (a, c) show result obtained with NUS schemes optimized only for the forward accordion experiment, while the right-hand panels (b, d) show the corresponding results obtained with schemes optimized individually for the forward and reverse accordion experiments. All data were acquired using adiabatic alignment.

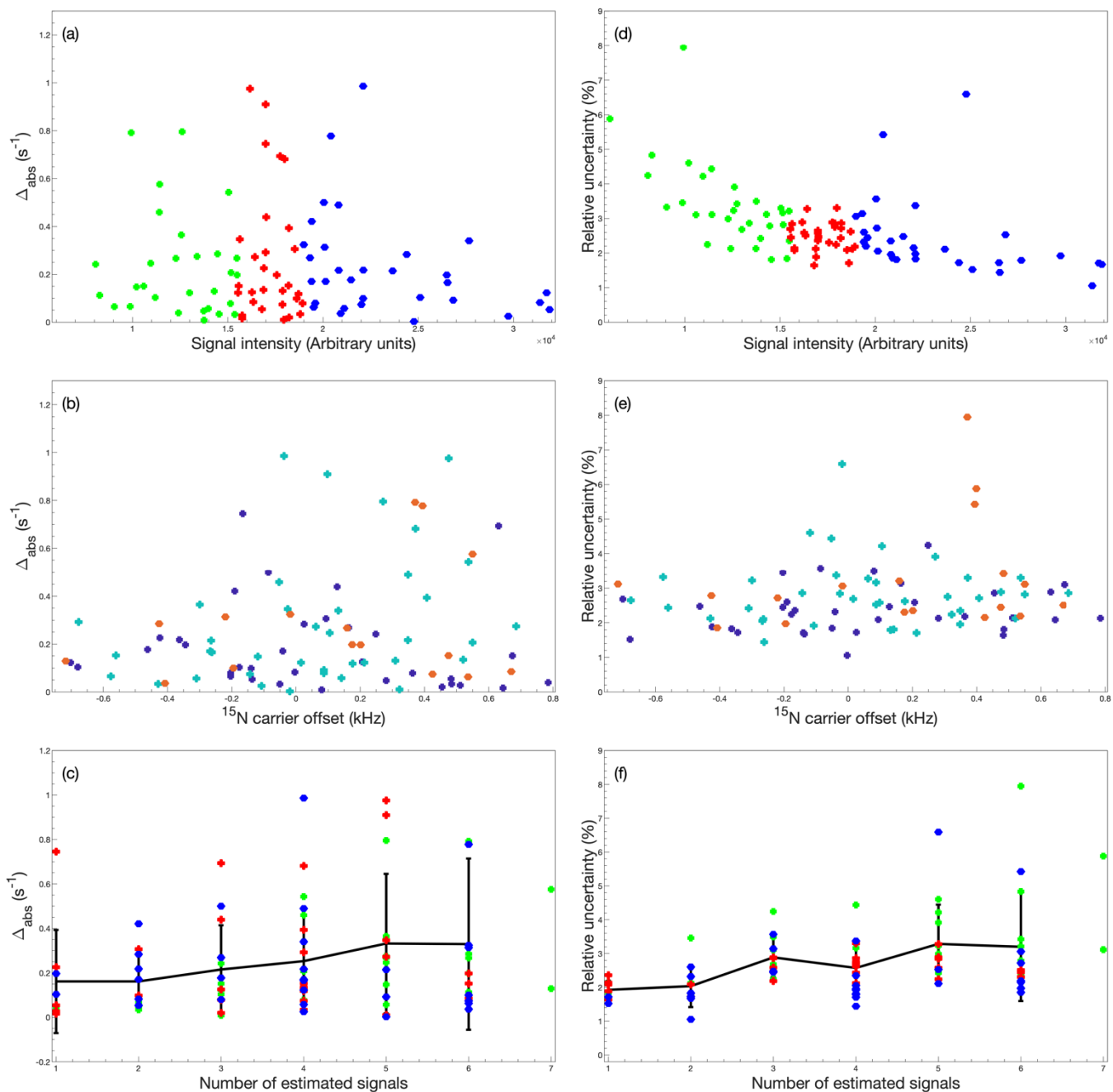
3.4 Spectral characteristics affecting accuracy and precision of accordion-NUS $R_{1\rho}$ relaxation rate constants

Next, we investigated how various spectral characteristics affect the accuracy and precision of the estimated relaxation rate constant. We calculated the absolute deviation (Δ_{abs}) between the US estimate and the 50% NUS estimate ($N = 66$), as well as the relative uncertainty, for each residue and plotted the results against signal intensity, resonance frequency offset from the

305 spin-lock carrier, and the number of estimated signals present in the interferogram of the col-opt and F+R optimized data (Fig. 4). There is no obvious relationship between Δ_{abs} and signal intensity, although larger values of Δ_{abs} ($> 0.4 \text{ s}^{-1}$) are not observed for the most intense signals (Fig. 4a). However, there is a trend towards lower relative uncertainty with higher signal intensity (Fig. 4d), where a value of 1.5% is observed for the strongest signals and 6–8% at the other extreme. The results further reveal that the number of signals in the interferogram has an effect on both Δ_{abs} and the relative uncertainty, with a trend toward
310 slightly larger errors as the number of signals increases (Figs. 4c, f); the relative uncertainty varies from 1.5% for single signals to 6–8% for the worst cases among interferograms containing 7 signals. Reassuringly, the mean relative uncertainty increases only slightly from 2% for single peaks to 3.2% for 7 peaks. Thus, there is no dramatic decrease in performance even at the highest number of signals. This effect of the number of signals also explains the apparent higher Δ_{abs} and higher relative uncertainty for residues with offsets around 0 and 500 Hz, because this region of the spectrum is the most crowded (Figs. 4b,
315 e). Furthermore, this result mirrors the observations of deviations between the accordion and conventional data discussed above in connection with Fig. 2.

4 Conclusions

We have described a non-uniformly sampled accordion $R_{1\rho}$ experiment that complements the previously presented accordion-NUS R_1 experiment (Carlström et al., 2019). The present accordion-NUS $R_{1\rho}$ experiment allows accurate and precise
320 measurement of the transverse relaxation rate constant R_2 , while reducing sampling of the indirect dimension by at least 50%. The combination of accordion relaxation rate measurements with NUS achieves time saving of an order of magnitude compared to conventional experiments, in keeping with previous results presented for the corresponding accordion-NUS R_1 experiment (Carlström et al., 2019). In addition to on-resonance R_2 measurements, demonstrated herein, we anticipate that this experiment will be useful for on- and off-resonance $R_{1\rho}$ experiments to characterize chemical exchange processes. The
325 accordion-NUS approach has broad applications in heteronuclear relaxation studies; with suitable modifications, the pulse sequence reported here for backbone ^{15}N spins should be applicable to many other sites, e.g., ^{13}C spins.



330 **Figure 4.** Dependence of accordion-NUS $R_{1\rho}$ accuracy and precision on spectrum characteristics. (a–c) Absolute deviation (Δ_{abs}) between
 $R_{1\rho}$ values obtained from US and 50% NUS data, and (d–f) relative uncertainty ($\sigma_i/R_{1\rho,i}$) of $R_{1\rho}$ values obtained from 50% NUS data, plotted
as a function of (a, d) signal intensity, (b, e) ^{15}N spin-lock carrier offset, and (c, f) number of estimated signals in the interferogram. In panels
a, c, d, and f, the data are divided into tertiles according to signal intensity and color coded as: green, first tertile (lowest intensity); red,
335 second tertile; blue, third tertile. In panels b and e, the data are divided into subsets according to the number of estimated signals in the
interferogram and color coded as: purple, 1, 2, or 3 signals; cyan, 4 or 5 signals; orange, 6 or 7 signals. The black symbols with error bars in

panels (e) and (f) represent the average and standard deviation of all data with a given number of peaks in the interferogram. All data were acquired using adiabatic alignment and determined using col-opt and F+R optimized NUS schemes.

Code and data availability

Backbone chemical shift assignments have been deposited at Biological Magnetic Resonance Bank with the accession code:
340 50283. The NMR pulse sequences, relaxation data sets, and extracted relaxation rate constants are available at Mendeley Data together with MATLAB scripts implementing the DSURE algorithm (<https://doi:10.17632/zyryxrgkc3.1>).

Author contributions

SW, GC and MA conceived the overall experimental approach and designed pulse sequences; AJ contributed the DSURE algorithm and designed the analysis protocol together with GC; SW and GC performed experiments; SW, GC and MA analyzed
345 data; all authors contributed to writing the manuscript.

Competing interests

The authors declare that they have no conflict of interest.

Acknowledgments

This research was supported by the Swedish Research Council 2018-4995 and the Swedish SRA eSENCE 2020 6:2.

350 References

- Ahlner, A., Carlsson, M., Jonsson, B. H. and Lundström, P.: PINT: A software for integration of peak volumes and extraction of relaxation rates, *J. Biomol. NMR*, 56, 191–202, doi:10.1007/s10858-013-9737-7, 2013.
- Akke, M. and Palmer, A. G.: Monitoring Macromolecular Motions on Microsecond–Millisecond Time Scales by R1ρ–R1 Constant-Relaxation-Time NMR Spectroscopy, *J. Am. Chem. Soc.*, 118, 911–912, 1996.
- 355 Alderson, T. R. and Kay, L. E.: Unveiling invisible protein states with NMR spectroscopy, *Curr. Opin. Struct. Biol.*, 60, 39–49, doi:10.1016/j.sbi.2019.10.008, 2020.
- Bodenhausen, G. and Ernst, R. R.: The accordion experiment, a simple approach to three-dimensional NMR spectroscopy, *J. Magn. Reson.*, 45(2), 367–373, doi:10.1016/0022-2364(81)90137-2, 1981.
- Bodenhausen, G. and Ernst, R. R.: Direct determination of rate constants of slow dynamic processes by two-dimensional
360 “accordion” spectroscopy in nuclear magnetic resonance, *J. Am. Chem. Soc.*, 104, 1304–1309, 1982.
- Bodenhausen, G. and Ruben, D. J.: Natural abundance nitrogen-15 NMR by enhanced heteronuclear spectroscopy, *Chem.*

- Phys. Lett., 69, 185–189, 1980.
- Carlström, G., Elvander, F., Swärd, J., Jakobsson, A. and Akke, M.: Rapid NMR relaxation measurements using optimal nonuniform sampling of multidimensional accordion data analyzed by a sparse reconstruction method, *J. Phys. Chem. A*, 123, 5718–5723, doi:10.1021/acs.jpca.9b04152, 2019.
- Carr, P. A., Fearing, D. A. and Palmer, A. G.: 3D Accordion Spectroscopy for Measuring ^{15}N and ^{13}CO Relaxation Rates in Poorly Resolved NMR Spectra, *J. Magn. Reson.*, doi:10.1006/jmre.1998.1374, 1998.
- Chen, K. and Tjandra, N.: Direct measurements of protein backbone ^{15}N spin relaxation rates from peak line-width using a fully-relaxed Accordion 3D HNCO experiment, *J. Magn. Reson.*, 197, 71–76, doi:10.1016/j.jmr.2008.12.001, 2009.
- Davis, D. G., Perlman, M. E. and London, R. E.: Direct measurements of the dissociation-rate constant for inhibitor-enzyme complexes via the T1 ρ and T2 (CPMG) methods, *J. Magn. Reson. Ser. B*, 104, 266–275, 1994.
- Delaglio, F., Grzesiek, S., Vuister, G. W., Zhu, G., Pfeifer, J. and Bax, A.: NMRPipe: A multidimensional spectral processing system based on UNIX pipes, *J. Biomol. NMR*, 6, 277–293, 1995.
- Diehl, C., Genheden, S., Modig, K., Ryde, U. and Akke, M.: Conformational entropy changes upon lactose binding to the carbohydrate recognition domain of galectin-3, *J. Biomol. NMR*, 45, 157–169, doi:10.1007/s10858-009-9356-5, 2009.
- Diehl, C., Engström, O., Delaine, T., Håkansson, M., Genheden, S., Modig, K., Leffler, H., Ryde, U., Nilsson, U. J. and Akke, M.: Protein flexibility and conformational entropy in ligand design targeting the carbohydrate recognition domain of galectin-3, *J. Am. Chem. Soc.*, 132, 14577–14589, 2010.
- East, K. W., Delaglio, F. and Lisi, G. P.: A simple approach for reconstruction of non-uniformly sampled pseudo-3D NMR data for accurate measurement of spin relaxation parameters, *J Biomol NMR*, doi:10.1007/s10858-021-00369-7, 2021.
- Farrow, N. A., Zhang, O., Forman-Kay, J. D. and Kay, L. E.: Comparison of the backbone dynamics of a folded and an unfolded SH3 domain existing in equilibrium in aqueous buffer, *Biochemistry*, 34, 868–878, 1995.
- Gołowicz, D., Kasprzak, P., Orekhov, V. and Kazimierczuk, K.: Fast time-resolved NMR with non-uniform sampling, *Prog. Nucl. Magn. Reson. Spectrosc.*, doi:10.1016/j.pnmrs.2019.09.003, 2020.
- Grzesiek, S. and Bax, A.: The importance of not saturating H $_2$ O in protein NMR. Application to sensitivity enhancement and NOE measurements, *J. Am. Chem. Soc.*, 115, 12593–12594, 1993.
- Hansen, D. F. and Kay, L. E.: Improved magnetization alignment schemes for spin-lock relaxation experiments, *J. Biomol. NMR*, 37(4), 245–255, doi:10.1007/s10858-006-9126-6, 2007.
- Harden, B. J. and Frueh, D. P.: SARA: A software environment for the analysis of relaxation data acquired with accordion spectroscopy, *J. Biomol. NMR*, 58(2), 83–99, doi:10.1007/s10858-013-9807-x, 2014.
- Hyberts, S. G., Takeuchi, K. and Wagner, G.: Poisson-gap sampling and forward maximum entropy reconstruction for enhancing the resolution and sensitivity of protein NMR data, *J. Am. Chem. Soc.*, 132(7), 2145–2147, doi:10.1021/ja908004w, 2010.
- Hyberts, S. G., Arthanari, H., Robson, S. A. and Wagner, G.: Perspectives in magnetic resonance: NMR in the post-FFT era, *J. Magn. Reson.*, 241(1), 60–73, doi:10.1016/j.jmr.2013.11.014, 2014.

- Jameson, G., Hansen, A. L., Li, D., Bruschweiler-Li, L. and Brüschweiler, R.: Extreme Nonuniform Sampling for Protein NMR Dynamics Studies in Minimal Time, *J. Am. Chem. Soc.*, 141(42), 16829–16838, doi:10.1021/jacs.9b08032, 2019.
- Juhlin, M., Elvander, F., Sward, J. and Jakobsson, A.: Fast Gridless Estimation of Damped Modes, in *ISPACS 2018 - 2018 International Symposium on Intelligent Signal Processing and Communication Systems*, pp. 346–351., 2018.
- 400 Kay, L. E., Nicholson, L. K., Delaglio, F., Bax, A. and Torchia, D. A.: Pulse sequences for removal of the effects of cross correlation between dipolar and chemical-shift anisotropy relaxation mechanisms on the measurement of heteronuclear T1 and T2 values in proteins, *J. Magn. Reson.*, 97, 359–375, 1992a.
- Kay, L. E., Keifer, P. and Saarinen, T.: Pure absorption gradient enhanced heteronuclear single quantum correlation spectroscopy with improved sensitivity, *J. Am. Chem. Soc.*, 114, 10663–10665, 1992b.
- 405 Korzhnev, D. M., Tischenko, E. V and Arseniev, A. S.: Off-resonance effects in ¹⁵N T2 CPMG measurements, *J. Biomol. NMR*, 17, 231–237, 2000.
- Linnet, T. E. and Teilum, K.: Non-uniform sampling of NMR relaxation data, *J. Biomol. NMR*, 64(2), 165–173, doi:10.1007/s10858-016-0020-6, 2016.
- Loria, J. P., Rance, M. and Palmer, A. G.: A relaxation-compensated Carr-Purcell-Meiboom-Gill sequence for characterizing
410 chemical exchange by NMR spectroscopy, *J. Am. Chem. Soc.*, 121, 2331–2332, 1999.
- Mandel, A. M. and Palmer, A. G.: Measurement of relaxation rate constants using constant-time accordion heteronuclear NMR spectroscopy, *J. Magn. Reson. Ser. A*, 110, 62–72, 1994.
- Månsson, A., Jakobsson, A. and Akke, M.: Multidimensional Cramér-Rao lower bound for non-uniformly sampled NMR signals, in *European Signal Processing Conference*, pp. 974–978., 2014.
- 415 Massi, F., Johnson, E., Wang, C., Rance, M. and Palmer, A. G.: NMR R1ρ Rotating-Frame Relaxation with Weak Radio Frequency Fields, *J. Am. Chem. Soc.*, 126(7), 2247–2256, doi:10.1021/ja038721w, 2004.
- Mayzel, M., Ahlner, A., Lundström, P. and Orekhov, V. Y.: Measurement of protein backbone ¹³C and ¹⁵N relaxation dispersion at high resolution, *J. Biomol. NMR*, 69(1), 1–12, doi:10.1007/s10858-017-0127-4, 2017.
- Mittermaier, A. K. and Kay, L. E.: Observing biological dynamics at atomic resolution using NMR, *Trends Biochem. Sci.*,
420 doi:10.1016/j.tibs.2009.07.004, 2009.
- Mobli, M. and Hoch, J. C.: Nonuniform sampling and non-Fourier signal processing methods in multidimensional NMR, *Prog. Nucl. Magn. Reson. Spectrosc.*, 83, 21–41, doi:10.1016/j.pnmrs.2014.09.002, 2014.
- Morris, G. A. and Freeman, R.: Enhancement of nuclear magnetic signals by polarization transfer, *J. Am. Chem. Soc.*, 101, 760–762, 1979.
- 425 Mosteller, F. and Tukey, J. W.: *Data Analysis and Regression. A Second Course in Statistics*, Addison-Wesley, Reading, MA., 1977.
- Mulder, F. A. A., de Graaf, R. A., Kaptein, R. and Boelens, R.: An off-resonance rotating frame relaxation experiment for the investigation of macromolecular dynamics using adiabatic rotations, *J. Magn. Reson.*, 131(2), 351–357, 1998.
- Mulder, F. A. A., Skrynnikov, N. R., Hon, B., Dahlquist, F. W. and Kay, L. E.: Measurement of slow (microseconds-

430 milliseconds) time scale dynamics in protein side chains by ^{15}N relaxation dispersion NMR spectroscopy: Application to Asn and Gln residues in a cavity mutant of T4 lysozyme, *J. Am. Chem. Soc.*, 123, 967–975, 2001.

Niklasson, M., Otten, R., Ahlner, A., Andresen, C., Schlagnitweit, J., Petzold, K. and Lundström, P.: Comprehensive analysis of NMR data using advanced line shape fitting, *J. Biomol. NMR*, 69, 93–99, doi:10.1007/s10858-017-0141-6, 2017.

Palmer, A. G.: NMR characterization of the dynamics of biomacromolecules, *Chem. Rev.*, 104(8), 3623–3640, 435 doi:10.1021/cr030413t, 2004.

Palmer, A. G., Cavanagh, J., Wright, P. E. and Rance, M.: Sensitivity improvement in proton-detected two-dimensional heteronuclear correlation NMR spectroscopy, *J. Magn. Reson.*, 93, 151–170, 1991.

Palmer, A. G., Skelton, N. J., Chazin, W. J., Wright, P. E. and Rance, M.: Suppression of the effects of cross-correlation between dipolar and anisotropic chemical shift relaxation mechanisms in the measurement of spin-spin relaxation rates, *Mol.* 440 *Phys.*, 75, 699–711, 1992.

Press, W. H., Flannery, B. P., Teukolsky, S. A. and Vetterling, W. T.: Numerical Recipes. The Art of Scientific Computing, Cambridge University Press, Cambridge., 1986.

Rabier, P., Kieffer, B., Koehl, P. and Lefevre, J.-F.: Fast measurement of heteronuclear relaxation: frequency-domain analysis of NMR accordion spectroscopy, *Magn. Reson. Chem.*, 39, 447–456, 2001.

445 Skelton, N. J., Palmer, A. G., Akke, M., Kördel, J., Rance, M. and Chazin, W. J.: Practical aspects of two-dimensional proton-detected ^{15}N spin relaxation measurements, *J. Magn. Reson. Ser. B*, 102, 253–264, 1993.

Stetz, M. A. and Wand, A. J.: Accurate determination of rates from non-uniformly sampled relaxation data, *J. Biomol. NMR*, 65(3–4), 157–170, doi:10.1007/s10858-016-0046-9, 2016.

Swärd, J., Adalbjörnsson, S. I. and Jakobsson, A.: High resolution sparse estimation of exponentially decaying N-dimensional 450 signals, *Signal Processing*, 128, 309–317, doi:10.1016/j.sigpro.2016.04.002, 2016.

Swärd, J., Elvander, F. and Jakobsson, A.: Designing sampling schemes for multi-dimensional data, *Signal Processing*, 150, 1–10, 2018.

Urbańczyk, M., Nowakowski, M., Koźmiński, W. and Kazimierzczuk, K.: Joint non-uniform sampling of all incremented time delays for quicker acquisition in protein relaxation studies, *J. Biomol. NMR*, 68, 155–161, doi:10.1007/s10858-017-0115-8, 455 2017.

Verteramo, M. L., Ignjatović, M. M., Kumar, R., Wernersson, S., Wallerstein, J., Carlström, G., Chadimova, V., Ekberg, V., Leffler, H., Zetterberg, F., Logan, D. T., Ryde, U., Akke, M. and Nilsson, U. J. In preparation, 2021.

Wallerstein, J., Ekberg, V., Misini Ignjatović, M., Kumar, R., Caldararu, O., Peterson, K., Leffler, H., Logan, D. T., Nilsson, U. J., Ryde, U. and Akke, M.: Entropy–Entropy Compensation Between the Conformational and Solvent Degrees of Freedom 460 Fine-tunes Affinity in Ligand Binding to Galectin-3C, *JACS Au*, 1, 484–500, doi:10.1021/jacsau.0c00094, 2021.

Wang, A. C. and Bax, A.: Minimizing the effects of radio-frequency heating in multidimensional NMR experiments, *J. Biomol. NMR*, 3, 715–720, 1993.

Waudby, C. A., Burrige, C. and Christodoulou, J.: Optimal design of adaptively sampled NMR experiments for measurement

of methyl group dynamics with application to a ribosome-nascent chain complex, J Magn Reson, 326, 106937, 2021.

- 465 Yip, G. N. B. and Zuiderweg, E. R. P.: A phase cycle scheme that significantly suppresses offset-dependent artifacts in the R-2-CPMG N-15 relaxation experiment, J. Magn. Reson., 171, 25–36, 2004.

Appendix A

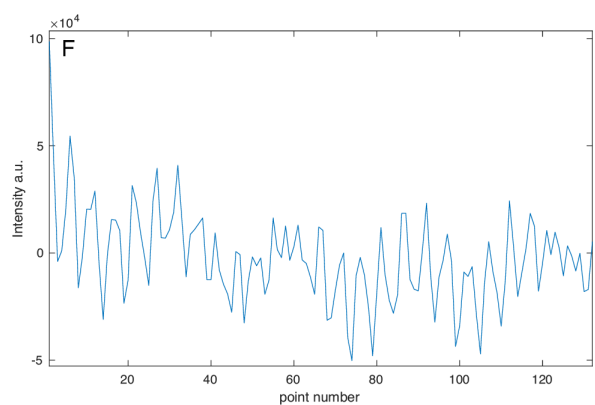
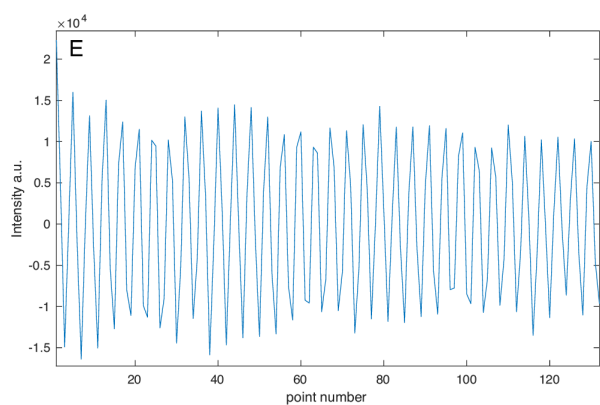
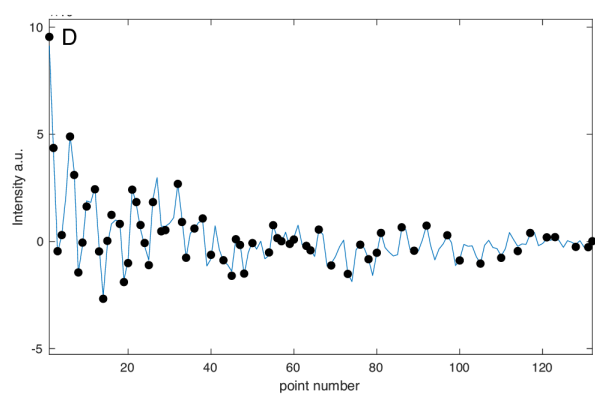
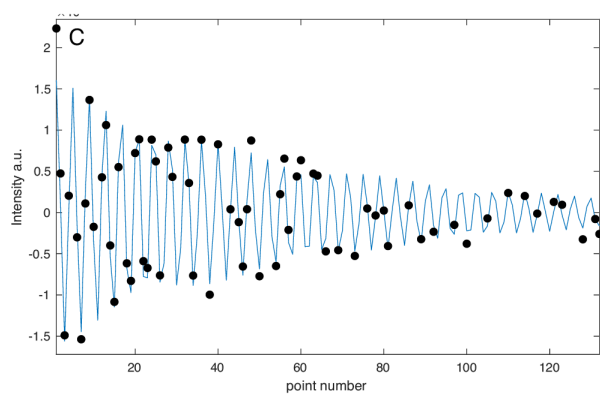
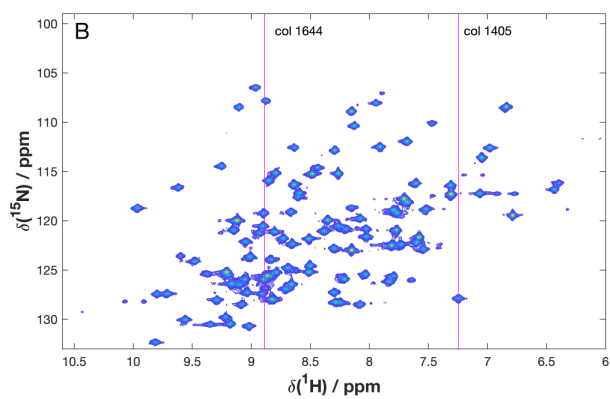
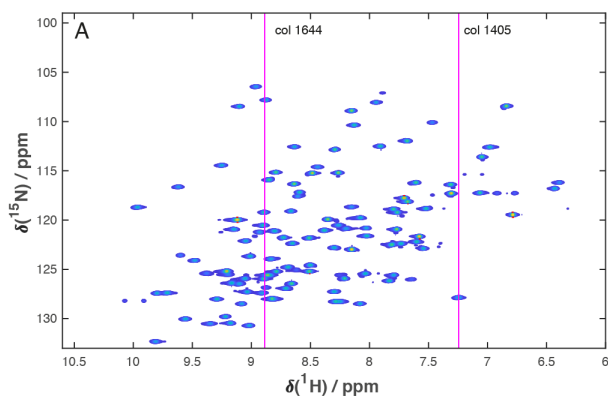


Figure A1. Representative accordion $R_{1\rho}$ datasets. (a, b) Full 2D ^1H - ^{15}N HSQC spectra from the (a) US reference experiment and (b) 50% NUS forward accordion experiment following DSURE reconstruction. The red lines identify columns 1405 containing a single peak and 1644 containing 8 peaks. (c, d) DSURE models of the interferograms of columns (c) 1405 and (d) 1644 extracted from the 50% NUS accordion experiment. The black dots indicate the sampled data points, while the blue curve shows the interferogram reconstructed by DSURE. (e, f) Interferograms of columns (e) 1405 and (f) 1644 extracted from the US reference experiment. Due to the constant time evolution period in t_1 , the interferograms in the reference experiment (e, f) show essentially no decay, whereas the interferograms in the accordion experiment (c, d) show significant decays due to the encoded $R_{1\rho}$ relaxation rate(s).

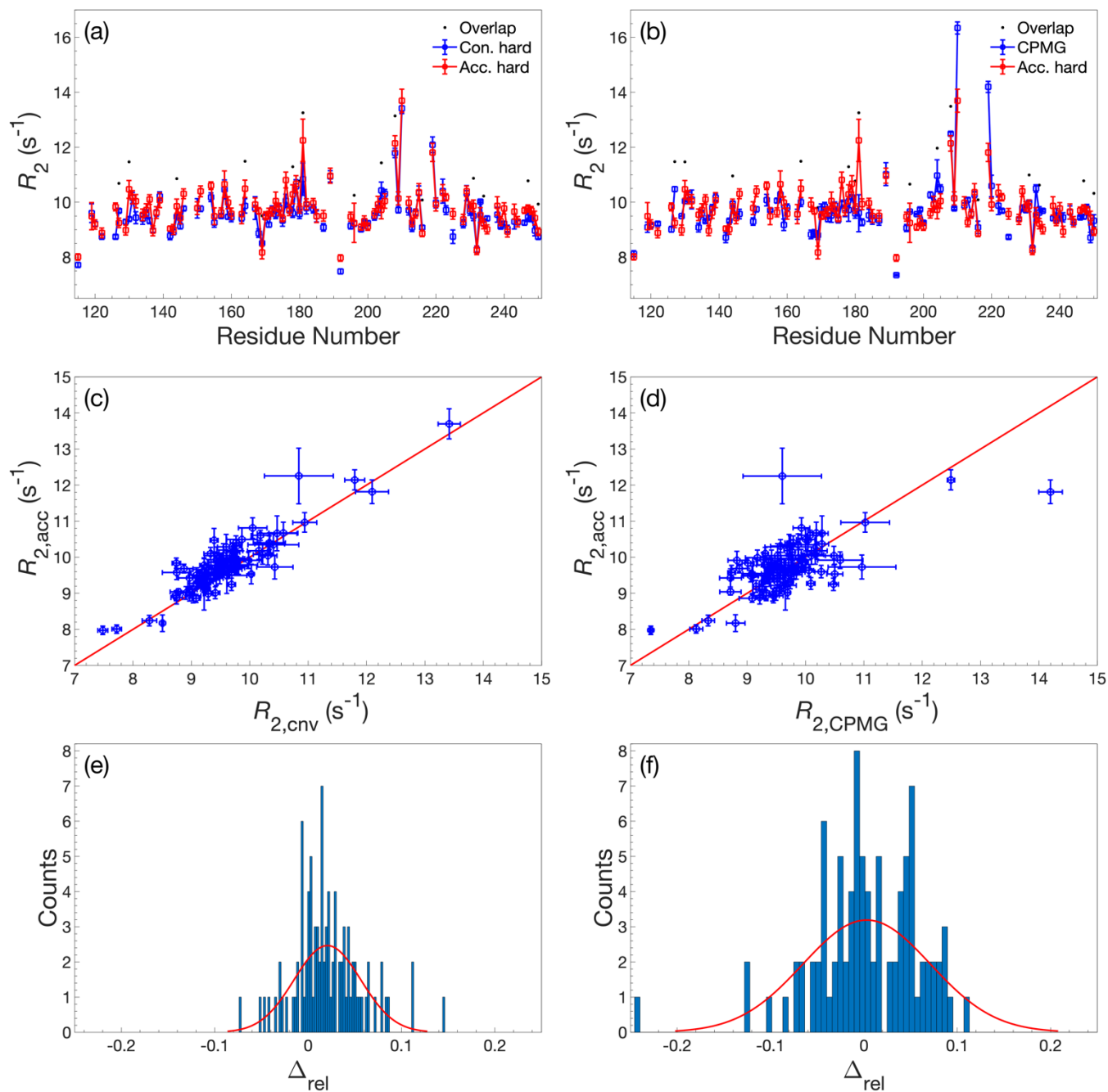
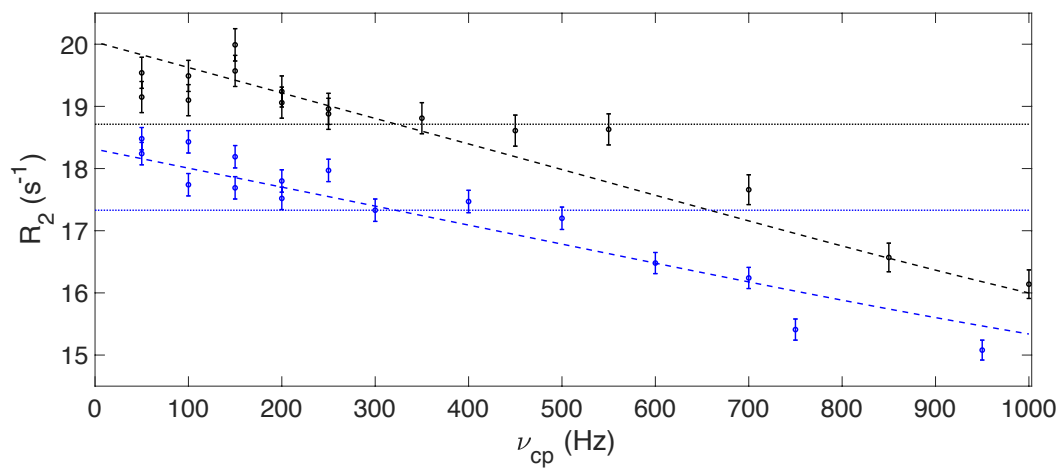
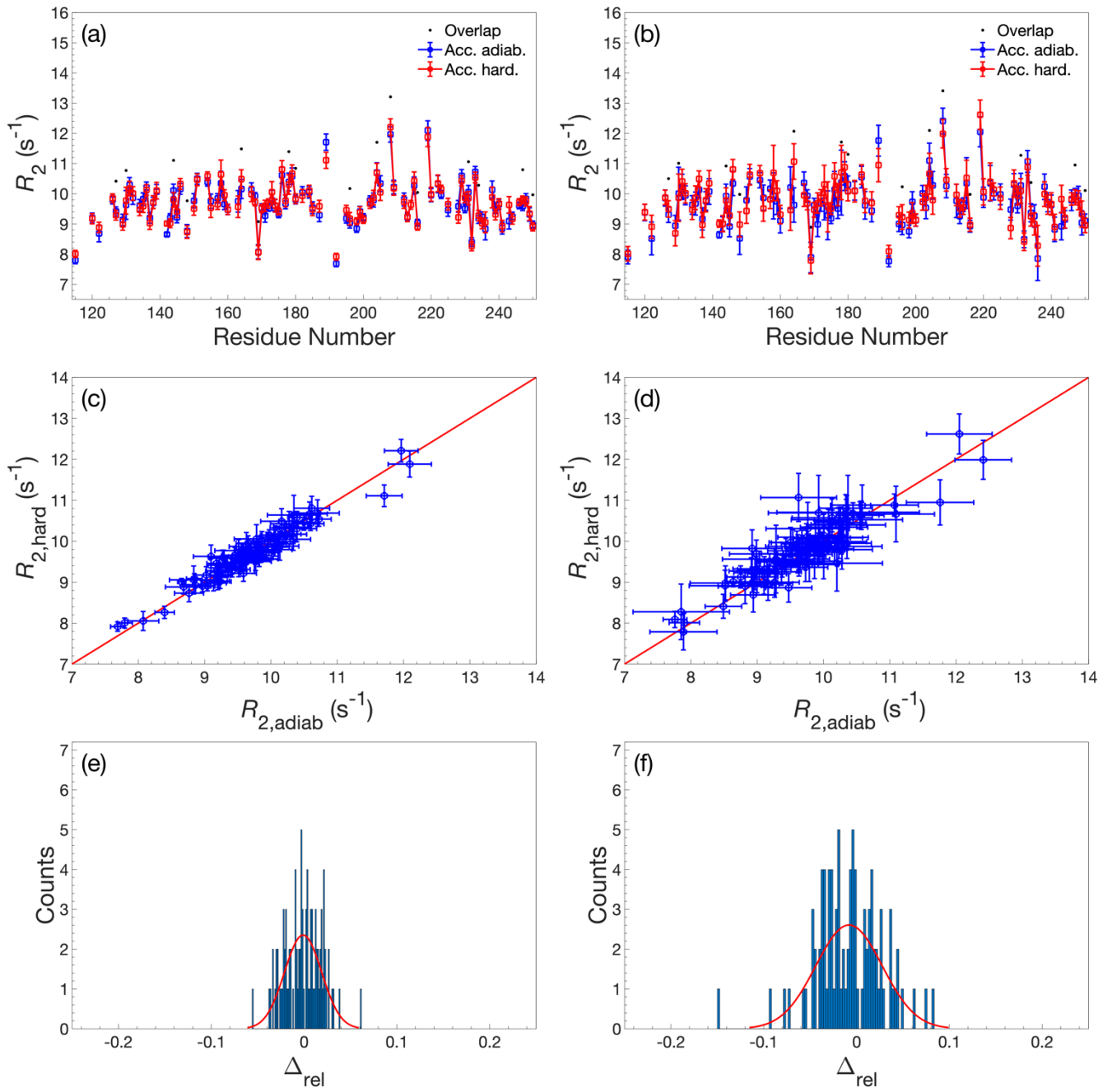


Figure A2. Comparison of R_2 determined by accordion $R_{1\rho}$ or conventional relaxation experiments. R_2 values determined by accordion $R_{1\rho}$ (red) spin-lock experiments compared with (a, c, e) R_2 determined by conventional $R_{1\rho}$ (blue) and (b, d, f) R_2 determined by conventional R_2 CPMG (blue). Both $R_{1\rho}$ experiments were acquired with hard-pulse alignment. (a, b) R_2 plotted versus residue number. Black dots indicate residues showing significant overlap in the ^1H - ^{15}N HSQC spectrum. (c, d) Covariance plot of R_2 datasets. (e, f) Histogram of the relative differences between datasets. The red curve describes the normal distribution that best fits the data. In panels (a–d), error bars indicate ± 1 SD.



490 **Figure A3.** CPMG relaxation dispersion profiles of residue L219, acquired at static magnetic field strengths of 11.7 T (blue) and 14.1 T (black). Dashed lines show the results of fitting a two-state exchange model globally to both data sets, which yielded an exchange rate of $7150 \pm 4100 \text{ s}^{-1}$, major state population of 0.99 ± 0.01 , and chemical shift difference of $7 \pm 4 \text{ ppm}$. The dotted horizontal lines show the average R_2 value at each field strength.

495



(Figure A4 continues on the next page)

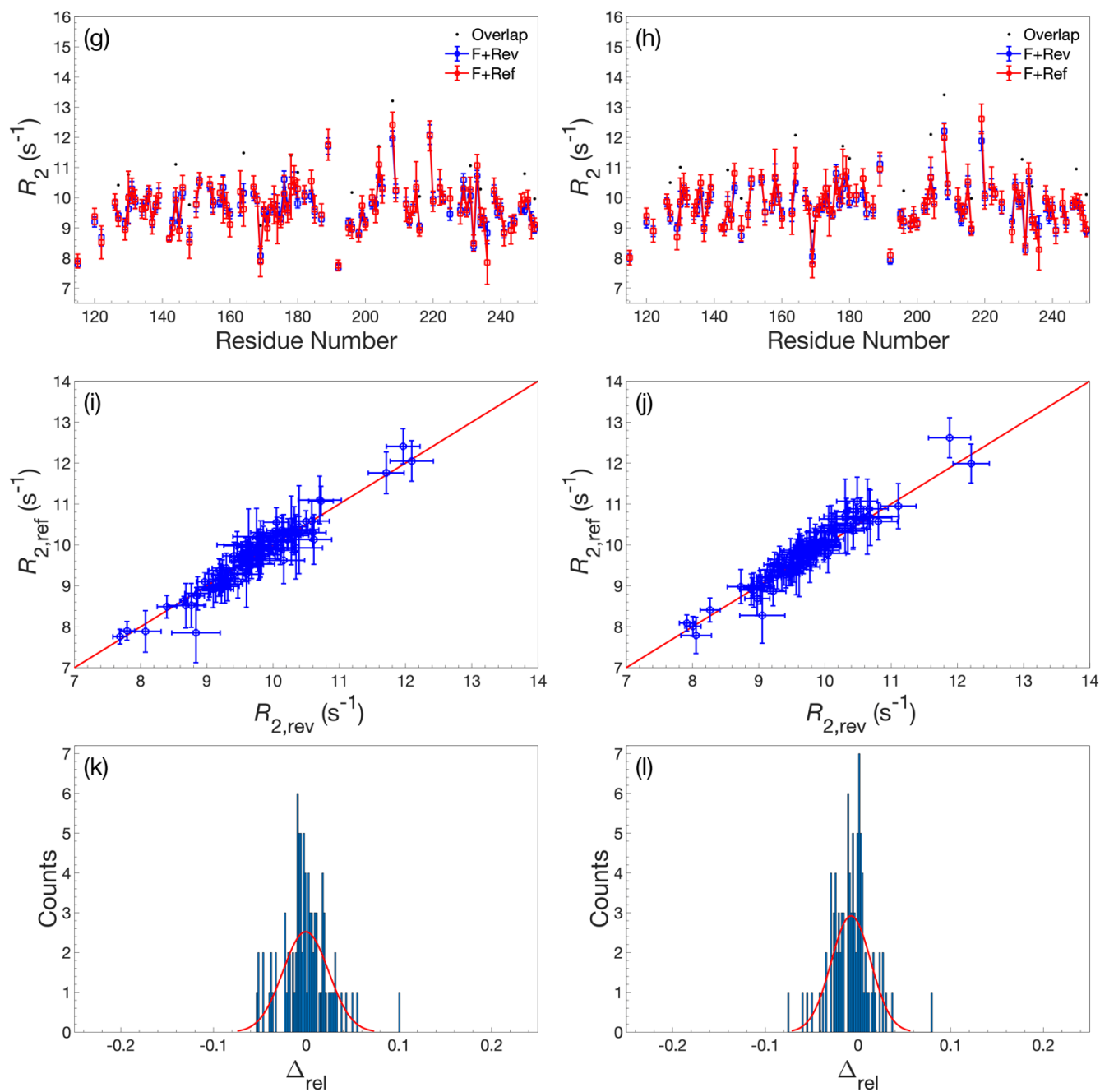


Figure A4. Comparison of R_2 determined by accordion $R_{1\rho}$ using various acquisition schemes. (a–f) Comparison of R_2 values determined using either adiabatic alignment (blue) or hard-pulse alignment (red). (g–l) Comparison of R_2 values determined using either forward–reverse (blue, F+Rev) accordion modes or forward–reference (red, F+Ref). (a, c, e) R_2 determined by forward–reverse accordion modes, (b, d, f) R_2 determined by forward–reference accordion modes. (a, b, g, h) R_2 plotted versus residue number. Black dots indicate residues showing significant overlap in the ^1H - ^{15}N HSQC spectrum. (c, d, i, j) Covariance plot of R_2 datasets. (e, f, k, l) Histogram of the relative differences between datasets. The red curve describes the normal distribution that best fits the data. In panels (a–d, g–j), error bars indicate ± 1 SD.